Automatic sequential fluid handling with multilayer microfluidic sample isolated pumping

Jixiao Liu, Hai Fu, Tianhang Yang, and Songjing Li[a)]
Department of Fluid Control and Automation, Harbin Institute of Technology, Harbin 150001, China

(Received 17 July 2015; accepted 21 September 2015; published online 1 October 2015)

To sequentially handle fluids is of great significance in quantitative biology, analytical chemistry, and bioassays. However, the technological options are limited when building such microfluidic sequential processing systems, and one of the encountered challenges is the need for reliable, efficient, and mass-production available microfluidic pumping methods. Herein, we present a bubble-free and pumping-control unified liquid handling method that is compatible with large-scale manufacture, termed multilayer microfluidic sample isolated pumping (mμSIP). The core part of the mμSIP is the selective permeable membrane that isolates the fluidic layer from the pneumatic layer. The air diffusion from the fluidic channel network into the degassing pneumatic channel network leads to fluidic channel pressure variation, which further results in consistent bubble-free liquid pumping into the channels and the dead-end chambers. We characterize the mμSIP by comparing the fluidic actuation processes with different parameters and a flow rate range of 0.013 μl/s to 0.097 μl/s is observed in the experiments. As the proof of concept, we demonstrate an automatic sequential fluid handling system aiming at digital assays and immunoassays, which further proves the unified pumping-control and suggests that the mμSIP is suitable for functional microfluidic assays with minimal operations. We believe that the mμSIP technology and demonstrated automatic sequential fluid handling system would enrich the microfluidic toolbox and benefit further inventions.
[http://dx.doi.org/10.1063/1.4932303]

I. INTRODUCTION

The field of microfluidics has yielded tons of technologies of novelty and inspiration, and at the same time, equivalent expectations have been given into this area for the last two decades. However, very few portions of developed technologies have been transformed into products, and the "killer application" has still not been unearthed. One of the encountered issues is that microfluidics has very limited technological options, especially fluidic actuation methods,[1–3] to build highly integrated and functional circuits to fulfill scientists' imaginations.

Microfluidic actuation is one of the core modules in a functional system, as all the other components are built on the chosen fluid handling method. Active fluidic actuation, such as pressure-driven,[4–7] centrifugal-based,[8] electrokinetic,[9,10] and acoustic[11] pumping, could finely control the liquid flow rate. However, they require costly and burdensome external equipment to build up a functional circuit. Additionally, such actuation methods are vulnerable to bubble formation and not suitable to load up dead-end structures that are attractive for quantitative digitized and multiplexed assays.[12–14] Most of the passive fluidic actuation methods lack effective positive control method or actuation reproducibility.[15–19] Take degas-driven flow as an example, it takes advantage of the Polydimethylsiloxane (PDMS) material to overcome the undesired bubble formation and enclosed chamber loading issue; however, it does not support

[a)]Author to whom correspondence should be addressed. Electronic mail: lisongjing@hit.edu.cn. Tel.: +86-451-86418318.

positive flow control during the pumping process and it is only effective in the device made of air-permeable materials.[18]

Undesired air bubbles in microfluidic devices are not rare for many applications and can enter a system through many processes such as liquid heating during PCR reaction thermocycling,[20,21] cell culture,[22,23] vacuum pressure driven flow, and directly introduced with the liquid during pumping.[24] Various strategies utilizing gas-permeable membranes[25–27] or porous structures[28,29] were invented in air bubble removal/trapping apparatuses. Yet, all of these developed techniques serve as assisted modules in addition to the liquid pumping equipment, not intrinsically built-in to the functions.

Microfluidic sequential flow devices have been developed for bioassays, such as pneumatic microvalve-based systems,[30–33] capillary-based systems,[34–40] the SlipChip systems,[41–43] and manual valving systems.[44] For most of these systems, liquid pumping process and flow control functions are separately driven by different accessory equipment, which ultimately increases the system complexity and the overall cost. And not all of these systems are able to process fluid samples in an automatic, controllable manner. Hence, new technological options for microfluidic sequential handling system are still necessary.

Here, we report a mass production feasible microfluidic liquid handling technology, named multilayer microfluidic sample isolated pumping (mμSIP). As depicted in Fig. 1, the mμSIP employs thermoplastics and silicone membranes as major materials to build the 3-D structures; hence, it is potentially available for industrial large-scale manufacture, which is of great importance for further commercialization. Also, it could provide bubble-free fluidic actuation and is feasible to dead-end structure loading. The liquid pumping and flow control can be achieved at the same time by one vacuum source when pneumatic microvalves are introduced. We illustrate the working principles and characterize the technology through experiments. We further demonstrate an automatic microfluidic sequential handling system based on mμSIP to prove the availability for potential bioassays. The mμSIP offers a new option for efficient, bubble-free liquid handling and also provides a new sight into building automatic microfluidic systems that enable high-density integrations and complex processing functions.

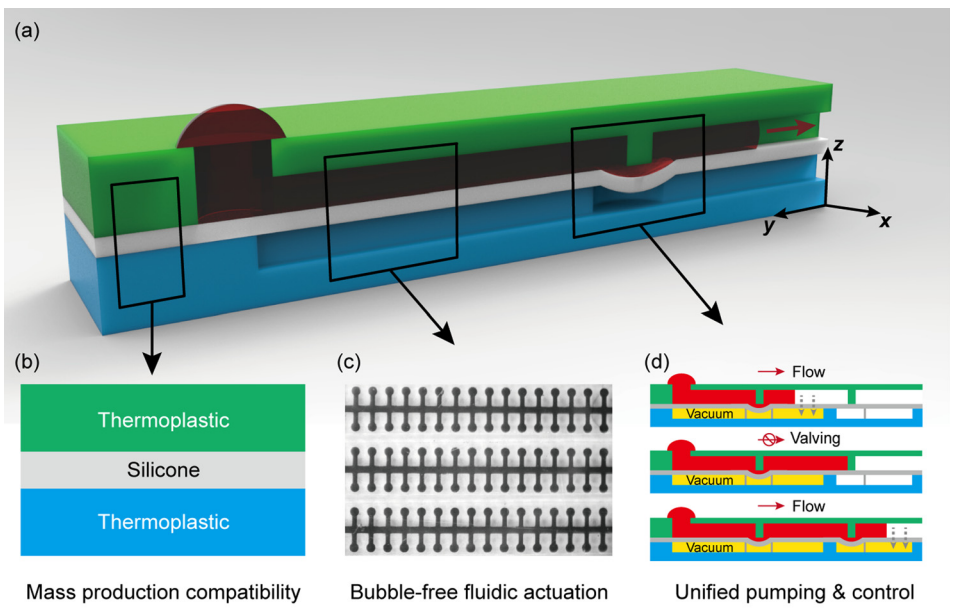

FIG. 1. Multilayer microfluidic sample isolated pumping (mμSIP). (a) and (b) The mμSIP device is made of thermoplastic and a silicone membrane, which makes it feasible for industrial large-scale production. (c) The mμSIP provides efficient and bubble-free liquid pumping for microfluidic assays and it is feasible for dead-end structure loading. (d) The mμSIP fluidic actuation is driven by vacuum pressure in the pneumatic layer, so by introducing pneumatic diaphragm microvalves into the structure, liquid pumping and flow control could be achieved at the same time in the device without extra accessory equipment.

II. WORKING PRINCIPLE OF MULTILAYER SAMPLE ISOLATED PUMPING

The main parts of the mμSIP are the fluidic layer, the pneumatic layer, and the middle layer of silicone membrane. These layers of structures are irreversibly bonded together, as shown in Figs. 1 and 2. In this paper, both the fluidic layer and pneumatic layer are fabricated using polystyrene (PS), and other materials that are compatible for irreversible bonding with silicone membranes can also be used to manufacture these two layers. During the implementation, the selectively permeable silicone membrane allows air (or other gases, but not aqueous solutions) to diffuse through and prevents the fluids from entering the pneumatic channels.

The fluidic channel network is an enclosed volume during liquid pumping and open outlets are not necessary, or the open outlets should be sealed during liquid flow. The channel network in the pneumatic layer is connected to a vacuum source when pumping, such as a vacuum pump or a finger pump.[45] When the vacuum is off, both the fluidic and pneumatic lines are at atmospheric pressure, as shown in Figs. 2(a) to 2(c), so no air diffusion or liquid flow occurs in the device.

When the vacuum pressure is exerted to the pneumatic channel network, there will be a pressure gradient between the liquid channel and the pneumatic channel across the silicone membrane, as fluidic channel pressure p_f is larger than pneumatic channel pressure p_d. Under the pressure gradient, the air in the fluidic channel diffuses into the degassing pneumatic channel through the membrane, as shown in Figs. 2(e) and 2(f). Under the consistent air mass

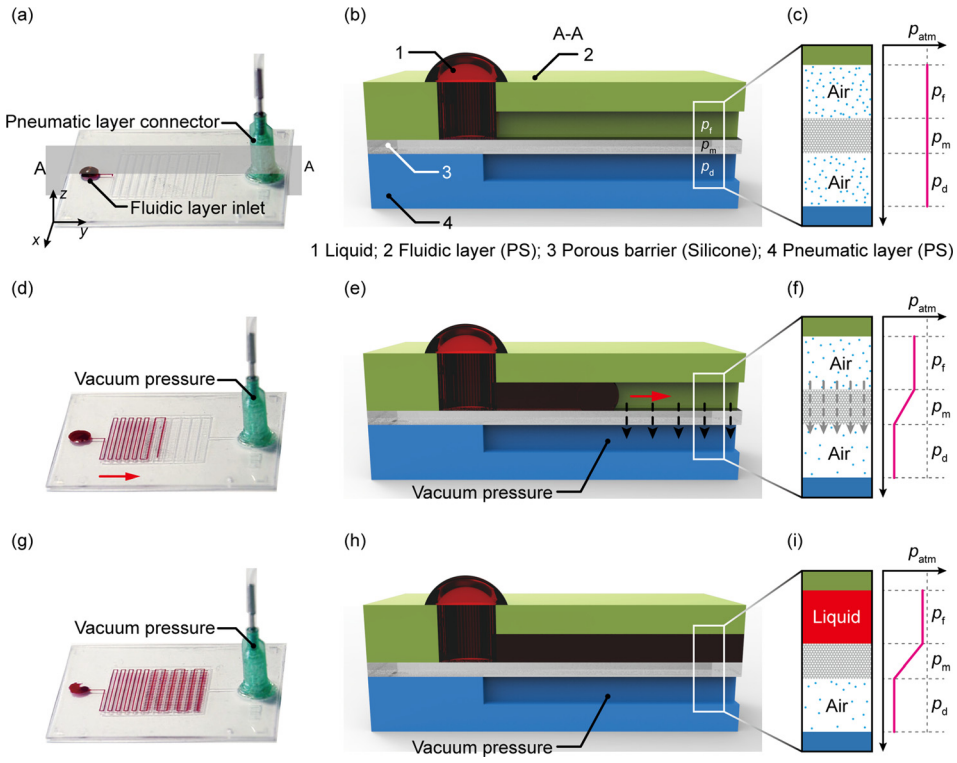

FIG. 2. The working principle of the multilayer microfluidic sample isolated pumping (mμSIP). (a) A device driven by mμSIP. Red liquid is pipetted into fluidic inlet. There is no outlet in the fluidic channel. (b) Cross-sectional view of part of the device. No vacuum is connected to the pneumatic channel, and no air diffusion or liquid flowing occurs. (c) Pressure conditions across the fluidic-membrane-pneumatic structure. Fluidic channel pressure p_f, pressure on the air-permeable membrane p_m, and the pneumatic channel p_d are equal to the atmospheric pressure. (d) and (e) Liquid starts to flow into the fluidic channel when vacuum is activated in pneumatic channels. Vacuum in the pneumatic lines leads to air diffusion from fluidic channel through the air-permeable membrane (dotted line arrows). The liquid cannot pass through the silicone membrane. The consistent air diffusion causes fluidic channel pressure reduction, which further drives liquid to flow into the channel. (f) Both of the fluidic channel pressure p_f and the pneumatic channel pressure p_d are below the atmospheric pressure. The pressure difference between the p_f and the p_d leads to the consistent air diffusion. (g), (h), (i) The fluidic channel is filled with the liquid. Air diffusion in the filled fluidic channel section is neglected.

transfer, the fluidic channel pressure decreases below the atmospheric pressure ($p_d < p_f < p_{atm}$). After overcoming the capillary pinning of the channel, the liquid flows into the fluidic channel under the pressure difference between the channel and the atmosphere. The consistent air evacuation from the fluidic channel leads to continuous fluid flow, until either channels/chambers are completely loaded or pressure equilibrium is reached.

When the flow proceeds into the further fluidic channel, the pressure in the liquid-filled channel sections varies, as shown in Figs. 2(h) and 2(i). The weak air mass transfer between the liquid and the pneumatic layer is neglected due to the poor air permeability of aqueous fluids.

The mμSIP liquid pumping is dependent on the air diffusion process between the fluidic channel network and the pneumatic channel network. Hence, it requires the geometrical pairing between the two networks. In an mμSIP device, the fluidic channel network is overlapped with or surrounded by the degassing pneumatic lines in close proximity in the *x*-*y* plane, while isolated from the degassing pneumatic lines in the *z* direction by the membrane, as shown in Figs. 2 and 3.

The working principle behind mμSIP allows inherently bubble-free fluidic actuation and eliminates any dead-volume within the microfluidic device. Besides, to use thermoplastics (PS, PC, PMMA, etc.) as the major materials would avoid some issues that are inevitable to the devices made of PDMS, such as leaching of uncured oligomers,[46] solution evaporation,[47] and small molecule absorption.[48] Also, these thermoplastic manufacturers are highly accessible in industries for high throughput manufacture, which makes this technology feasible for future commercialization. Still, it is highly functional and efficient for loading dead-end structures, while most of other microfluidic actuation methods are not able to achieve liquid sample loading in this way, especially in the microfluidic devices made of air-impermeable materials.

III. EXPERIMENTAL CHARACTERIZATIONS OF LIQUID PUMPING PROCESS

Microfluidic devices with different parameters were tested to demonstrate bubble-free liquid loading and to characterize the mμSIP fluidic actuation process, as shown in Fig. 3. All the microfluidic devices were fabricated with polystyrene and silicone membranes by a rapid prototyping protocol (see supplementary material).[53]

Fig. 3(a) illustrates one of the chip designs in the experimental characterizations. The fluidic channels and chambers are surrounded by pneumatic lines in the *x*-*y* plane in a close proximity. During the liquid pumping, the consistent outward air diffusion from the fluidic channel leaves no air bubble stuck inside, as demonstrated in Figs. 3(b) to 3(g), so the undesired air bubble formation can be fundamentally prevented in mμSIP devices, without any other assisted structure or equipment. Furthermore, the liquid could fill all the dead-end chambers within several minutes, which is potentially beneficial for microfluidic digital assays.

In the experiments, unless stated otherwise, the 100 μm-thick silicone membranes were used to isolate the fluidic and pneumatic layer in the *z* direction, and the vacuum pressure of −85 kPa (with respect to the atmospheric pressure) was exerted into the pneumatic degassing network during tests.

The air mass transfer into the pneumatic degas channel, which leads to fluidic channel pressure variation, is the driving force behind the liquid pumping. So based on Fick's 1st and 2nd law, ideal gas law, and Navier-Stoke equations, it could be inferred that for a certain fluidic channel network pattern, the major influential parameters in mμSIP devices are the silicone membrane thickness, the vacuum pressure in the pneumatic network during implementation, and the pneumatic channel coverage, as illustrated in Fig. 3(h). The theoretical equation derivation (Eqs. (S1) to (S6)) is developed to understand the multiphysical principles behind the fluidic actuation and to distinguish the major influential parameters (see supplementary material).[53]

The selective permeability of silicone membrane allows air to diffuse into the pneumatic channel from the fluidic channel under the concentration gradient. Hence, the Fick's 1st and 2nd laws suggest that the membrane thickness affects the air diffusion rate by influencing the air concentration gradient between the fluidic and pneumatic channels. Figs. 3(i) and 3(j) are the experimental comparison of liquid pumping with different membrane thicknesses under the

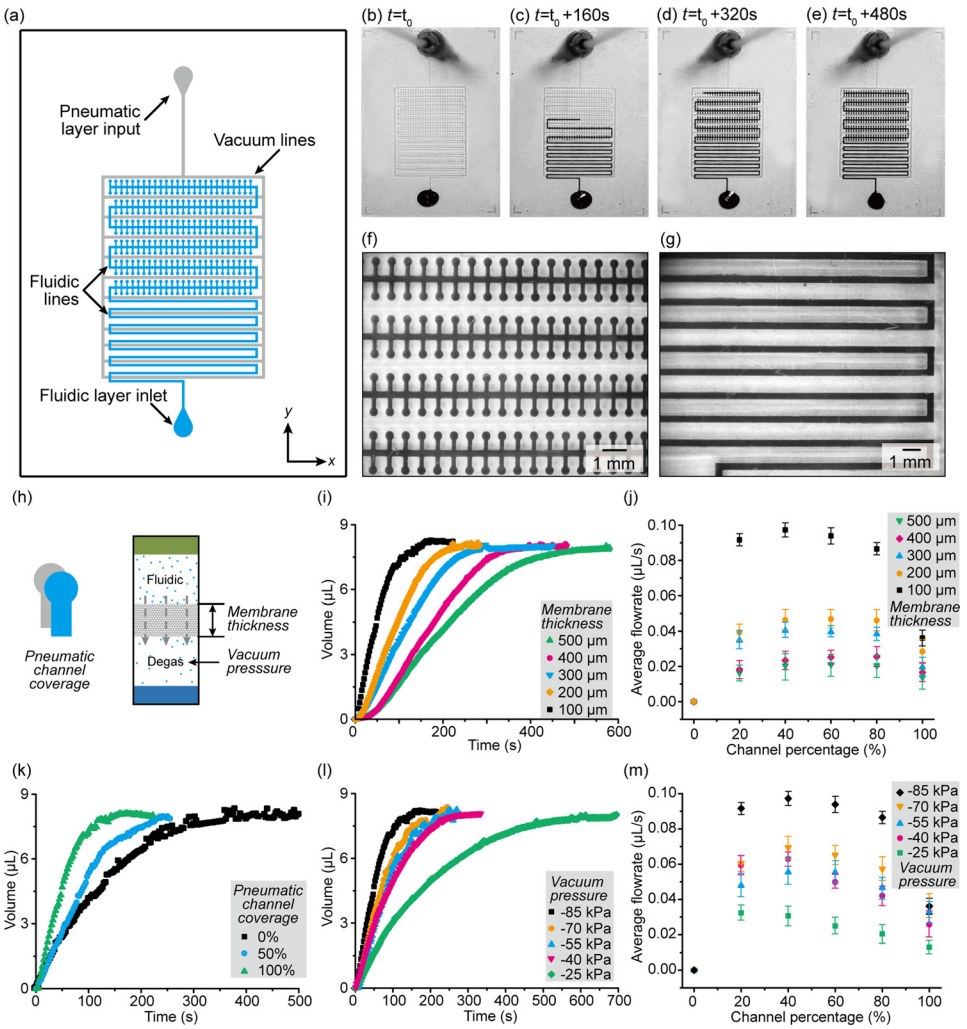

FIG. 3. Experimental characterizations of the mμSIP. (a) The basic chip design. Light-blue represents fluidic channels and chambers, and light-gray represents pneumatic lines. Three layers of structures are comprised in the device. (b)–(e) Liquid sample loading under −85 kPa in the pneumatic lines. No air bubbles observed. (f) and (g) Microscopic picture of dead-end chambers and channels after pumping. (h) Major parameters considered in the characterizations: the pneumatic channel coverage, the silicone membrane thickness, and the vacuum pressure. (i) and (j) Liquid pumping curves and average flow rate with different silicone membrane thickness under vacuum pressure of −85 kPa and with 100% pneumatic channel coverage. (k) Liquid pumping with different pneumatic channel coverage under vacuum pressure of −85 kPa and with 100 μm-thick silicone membrane. (l) and (m) Liquid pumping curves and average flow rate with different vacuum pressure with 100% pneumatic channel coverage and 100 μm-thick silicone membrane. Each test condition was repeated with three devices, only average data are plotted in the (i), (k), and (l). Unless stated otherwise, the 100 μm-thick silicone membranes, the vacuum pressure of −85 kPa (with respect to the atmospheric pressure), and 100% pneumatic channel coverage are applied in the tests.

same vacuum degassing pressure in the pneumatic channel. Silicone membranes with five different thicknesses, from 100 μm to 500 μm, were used in the test devices.

Fig. 3(i) plots the volume variations with different membranes during pumping. As the liquid flow curves at the beginning are much steeper compared with the latter part, it indicates that the liquid flows faster after initiation. Data also indicate that thicker silicone membrane leads to slower liquid pumping, because thicker membrane reduces the rate of air diffusion that results in smaller fluidic channel pressure variation and slower fluidic flow. Fig. 3(j) compares the average flow rates when different portions of the channels are filled with liquid. It suggests that when the liquid fills 20% to 80% of the fluidic channel, the standard deviations of average flow rates are less than 10% (except for the case of 500 μm, which is about 14.6%); therefore, the pumping between 20% and 80% completeness could be considered as quasi-steady and

consistent. Also, for the cases of thinner silicone membranes, such as 100 μm-thick membranes, the average flow rate deviations in this period are even smaller, compared to the cases of thicker membranes.

The pneumatic channel coverage is defined as the percentage of the overlapped area between the fluidic network and the pneumatic channels over the whole fluidic channel area in the *x-y* plane. For example, the coverage is defined as 0% for the design demonstrated in Fig. 3(a) and 100% when the fluidic channel is totally overlapped the pneumatic lines with the same network patterns in the *x-y* plane. Fig. 3(k) plots the liquid pumping curves with different coverages, as 0%, 50%, and 100%, separately. When the overlapped area increases, the air mass transfer is more efficient and the liquid pumping process runs faster since more air is evacuated from the fluidic channel in the same amount of time, such as the case of 100% coverage compared to the case of 0% coverage. Unless stated otherwise, the pneumatic channel coverage of the tested devices is 100%.

The vacuum pressure in the pneumatic lines initiates all the physical processes that occur during fluidic actuation. The influence of the vacuum pressure on the liquid pumping is shown in Figs. 3(l) and 3(m). Conditions with five different vacuum pressures were measured, from −25 kPa to −85 kPa (with respect to the atmospheric pressure), and for each condition, three devices were separately tested. Unsurprisingly, larger vacuum pressure, such as the case of −85 kPa (with respect to the atmospheric pressure), provides much faster liquid pumping, compared with the case of −25 kPa (with respect to the atmospheric pressure). Also, Fig. 3(m) suggests that the flow in the period of filling 20% to 80% of the fluidic channel is quite coherent, and the uniformity of flow rate is more obvious when the liquid flow is faster, which is also found in Fig. 3(j).

The characterizations suggest that the liquid flow is tunable by varying the parameters, and it could be approximately considered as consistent for the middle section of the fluidic channels. Also, as shown in Fig. 3, in the 20% to 80% section of the liquid channel loading, an average flow rate of 0.013 μl/s (in the case of 0% coverage, −85 kPa and 100 μm-thick) to 0.097 μl/s (in the case of 100% coverage, −85 kPa and 100 μm-thick) was observed in the characterizations.

IV. AUTOMATIC MICROFLUIDIC SEQUENTIAL HANDLING

Microfluidic sequential handling is the combination of efficient liquid pumping method and operational flow control technique. The existing sequential flow devices either introduce valving mechanisms into pumping systems, such as paper-based microfluidic circuits,[39,40] or build integrated micropumps based on the flow control structures, such as the Quake systems.[33] In our work, pneumatic diaphragm microvalves are integrated into an mμSIP device since both of the fluidic actuation and the diaphragm microvalves are built with multi-layer structures and driven by the vacuum pressure,[49] which is described as unified pumping and control.

Based on this unified liquid pumping-control feature, we invented an automatic microfluidic sequential handling system that could process multiple liquid samples and reagents based on the designed sequences, as shown in Fig. 4. The systems are comprised of two parts: the miniature pressure source and the microfluidic chips. The miniature pressure source consists of a DC power, a single-chip microcontroller, miniature relays, a miniature pressure pump, and miniature pneumatic switches, as shown in Figs. 4(a) and 4(b). The microfluidic chip is the core of the system, which could be a chip for digital bioassays or immunoassays, or any devices that are driven by mμSIP technique, as shown in Figs. 4(c) to 4(h).

In the miniature pressure source, the DC power converts AC (220 V) into DC (24 V and 5 V), and it could be a voltage transformer or a high capacity DC battery. In this work, a voltage transformer (220 V to 24 V, Xinying XY-005K-24V-1.5A, Guangzhou, China) and tunable step-down IC converter (24 V to 5 V, MP1584EN, D-Sun, Guangzhou, China) are used to build the DC power module. The control module, as the single-chip microcontroller (STC89C52, Shenzhen, China) and miniature relays (Omron G5V-1-5VDC, Shenzhen, China), is to control the on/off statuses of the miniature pneumatic switches that further decide which channels will be connected to the vacuum pressure from the pneumatic system. The pneumatic module, as

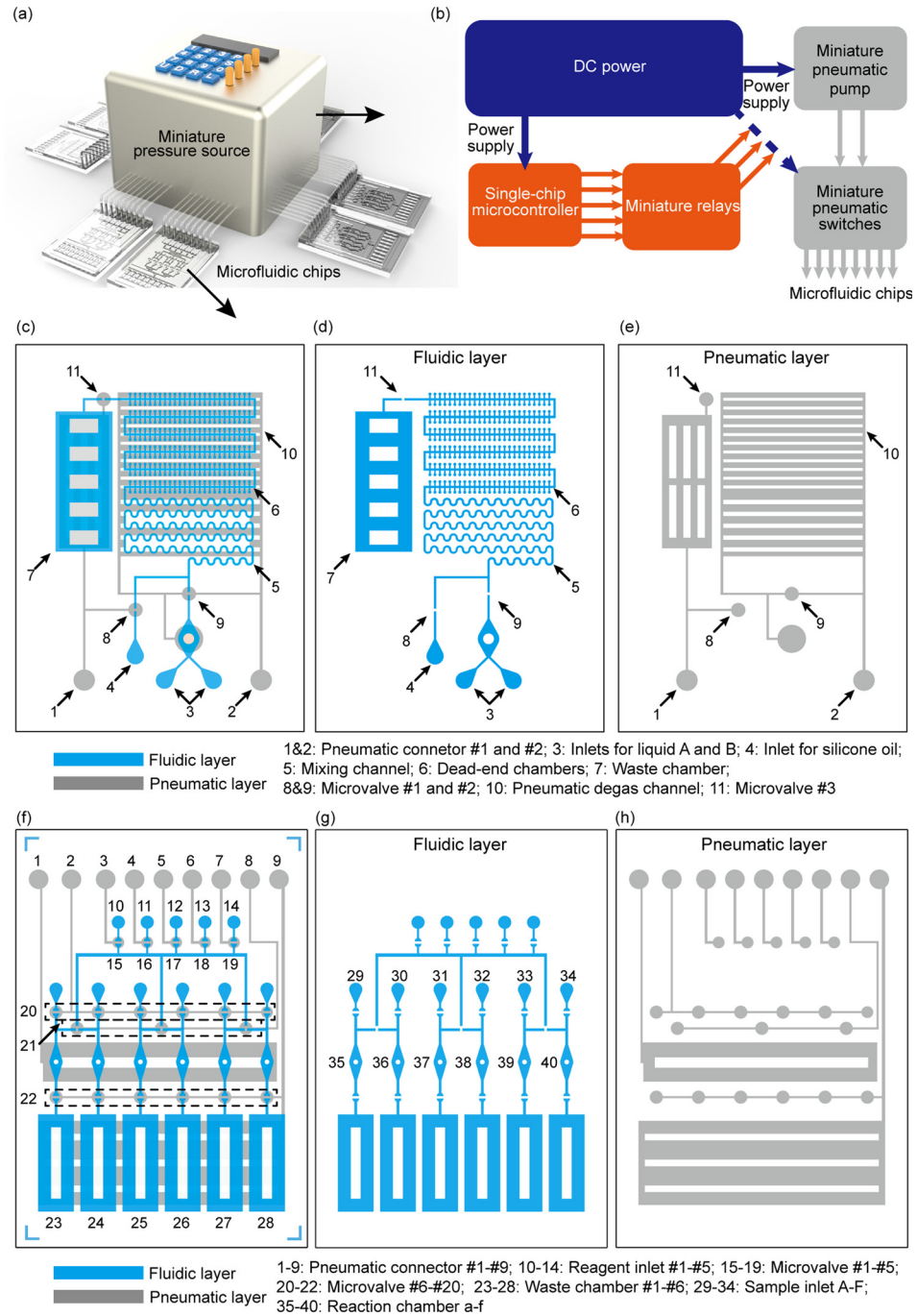

FIG. 4. The automatic microfluidic sequential handling system. (a) The schematics of the automatic microfluidic sequential handling system: the miniature pressure source and the microfluidic chips. (b) The design of the miniature pressure source. It consists of a DC power module, a control module, and a pneumatic module. (c) The design of the two-step sequential handling device for digital assays. (d) The fluidic layer pattern. (e) The pneumatic layer patter. (f) The design of the multiple-step sequential handling device for immunoassays. (g) The fluidic layer pattern. (h) The pneumatic layer patter.

the tunable miniature pressure pump (Kamoer KVP04, Shanghai, China) and the miniature pneumatic switches (Enja, DC6V, Xiamen, China), supplies positive or vacuum pressure to specific channels under the control from the control module.

Sequential processing of samples and reagents is essential to number of biochemical and biophysical applications. Here, in this paper, we demonstrate two different types of microfluidic

chips for sequential handling: a two-step sequential handling device aiming at potential digital bioassays and a multi-step sequential handling device aiming at potential immunoassays. The designs of these two devices are shown in Figs. 4(c) to 4(h), and the validation tests are demonstrated in Figs. 5 and 6 separately.

The two-step sequential handling device is designed for potential digital assays. It consists of inlets, mixing channels, dead-end chambers, a waste chamber, diaphragm microvalves,[49] and built-in mμSIP structures, as depicted in Fig. 4(c). In the fluidic layer illustrated in Fig. 4(d), three liquid samples, liquid A, liquid B, and silicone oil that is immiscible with A or B, are supplied. In the pneumatic layer, there are two branches of networks. For each step of operation, there is a branch of the pneumatic line being activated by the vacuum pressure to operate liquid loading and flow control at the same time, as illustrated in Fig. 4(e). The liquid loading is actuated by mμSIP and the flow control is operated by the pneumatic diaphragm microvalves under the same vacuum pressure in each branch of pneumatic channels. This unified pumping-control technique combines the flow control apparatus within the fluidic actuation structures to diminish the need for extra equipment or tubing.

The multiple-step sequential handling device is designed for potential immunoassays. It consists of inlets, reaction chambers, waste chambers, diaphragm microvalves, and built-in mμSIP structures, as shown in Fig. 4(f). The device could handle six different fluidic samples and five additional reagents in a seven-step procedure. To control the sequential flow, there are nine pneumatic channel lines to assist the fluidic network, as illustrated in Figs. 4(g) and 4(h). For each step, there is a pneumatic branch being activated to drive the liquid pumping and to switch the microvalves simultaneously.

As proofs of concept, both of the devices are tested with colored dye solutions and DI water in the validation demonstration, instead of biological or chemical samples, as shown in Figs. 5 and 6.

A. A two-step sequential handling device for digital bioassays

Microfluidic digital assays have become attractive in quantitative nucleic acid analysis nowadays, and the dead-end structure liquid loading and the reaction chamber digitization are crucial during the nucleic acid amplification and the following quantification.[14,50–52] As shown in Figs. 4 and 5, the two-step microfluidic sequential handling device demonstrated in this paper is capable of handling sample mixing, dead-end chamber loading, and fully digitization within only two steps of operations.

The first step is to mix and load liquids into the dead-end reaction chambers, as demonstrated in Fig. 5(a). Both liquid A (in red) and liquid B (in blue) are pipetted into the inlets (#3 in Fig. 4(c)), then the first pneumatic line is activated by a vacuum pressure of −85 kPa (with respect to the atmospheric pressure) to switch on the microvalve (#9) and to drive the liquids flowing into the channel. The serpentine curve-shape channel accelerates the mixing process between A and B by cross-sectional secondary flow, and as the result, the liquid color turns into dark purplish from red or blue, as shown in Figs. 5(a)(i) and 5(a)(ii). When it proceeds in the main "bus" channel, the mixed liquid is being loaded into the dead-end chambers, which locate along the "bus" channel on each side, as in Figs. 5(a)(iii) to 5(a)(vi). The vacuum pressure in the pneumatic lines keeps degassing the fluidic channel, so all the air in the fluidic lines/chambers is evacuated and the fluidic channel is free of air bubble at last, as shown in Fig. 5(a)(vi).

After the chambers are fully loaded with mixed liquid, the second pneumatic line is activated by vacuum pressure source and the microvalves (#8, #11) are switched on. The first pneumatic branch is turned off. The remained solution in the main "bus" channel (not the solution in the dead-end chambers) proceeds into the waste chamber (#7), and at the same time, the immiscible silicone oil in inlet #4 flows into the main channel to digitize these enclosed chambers, as shown in Figs. 5(b)(i) to 5(b)(iv). Due to the surface tension between the aqueous solution and the silicone oil, when the oil flows by the chambers, it seals the chamber entrances by the solution-oil interfaces and the aqueous solution in the dead-end chambers cannot trespass. In

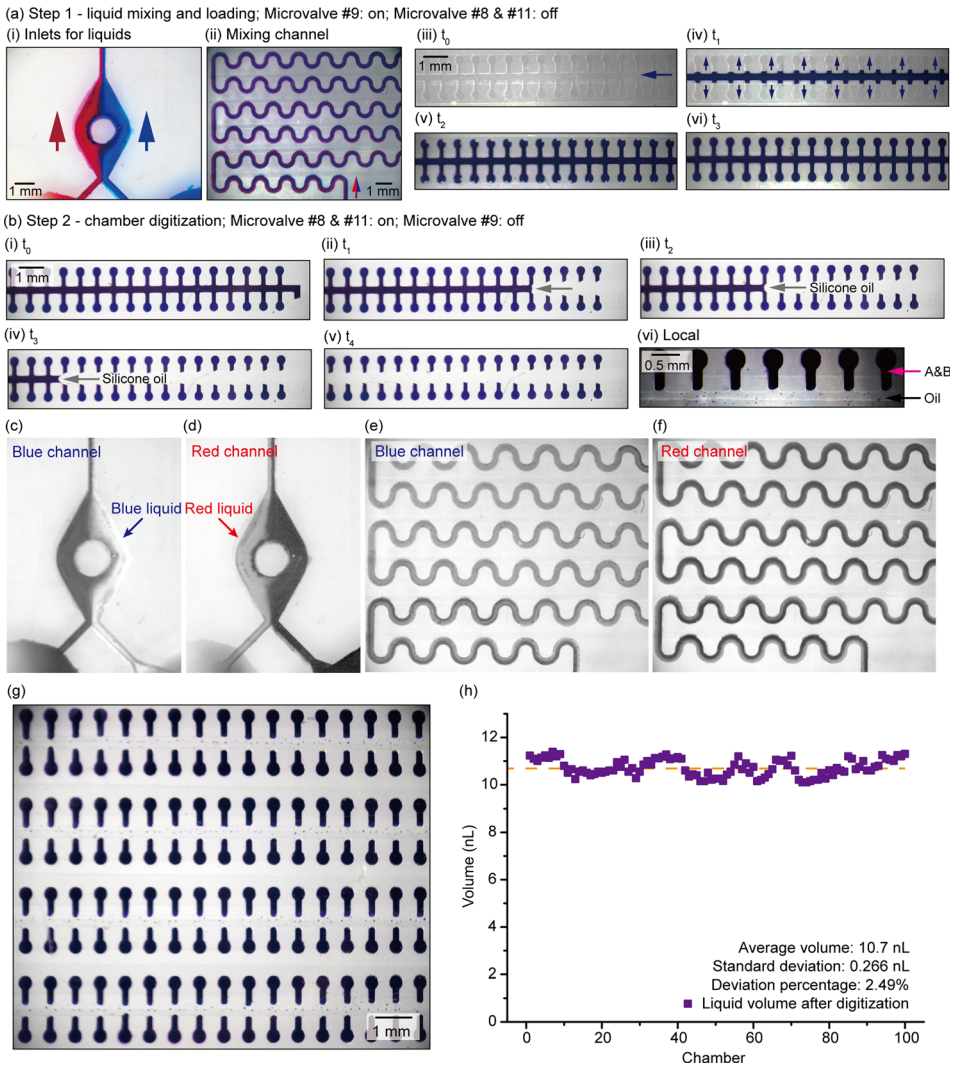

FIG. 5. Experimental test and evaluation of the two-step sequential handling device. (a) Liquid mixing and dead-end chambers loading. The first pneumatic line is exerted with vacuum pressure. (i) Liquids A and B are loaded into the channel at the same time. (ii) Liquids are mixed in the serpentine curved channel and the solution turns to dark blue-purplish at the end of the channel. (iii) and (iv) The dead-end chambers start to load the mixed solution. (v) and (vi) Air is evacuated from the chambers and all the dead-end chambers are fully loaded at the end. (b) Chamber digitization. The second pneumatic line is switched on. The silicone oil flows into the channel to separate the chambers to accomplish digitization. The chambers are sealed with the silicone oil and cannot contact with each other during further operations. (c) and (d) Blue and red intensities at the inlet that are analyzed by Adobe Photoshop. Brighter area in the color channel represents more concentrated liquids of that color. (e) and (f) Blue and red intensities in the serpentine mixing channel that are analyzed by Adobe Photoshop. Both color intensities become uniform in the latter section of the mixing channel, which indicates the uniform mixing. (g) Chambers after fully digitalization. (h) Measurement of liquid volume in one hundred digitized chambers. Deviations of liquid volume among chambers are minor compared to the average value (see details in supplementary material).[53]

this way, the dead-end chambers are well isolated from each other to achieve fully digitization, as shown in Figs. 5(b)(v) and 5(b)(vi).

Evaluation of the mixing intensity and the following digitalization are depicted in Figs. 5(c) to 5(h). During the device operation, red and blue liquids are mixed in the serpentine curved channel. The microscopic pictures were analyzed in Adobe Photoshop software (Adobe, Inc.) by isolating the blue and red channels from the overall RGB distribution, as shown in Figs. 5(c) to 5(f), to compare the mixing intensity variation during liquid flow. In each color channel, brighter areas represent more concentrated liquids in that color, for example, the bright

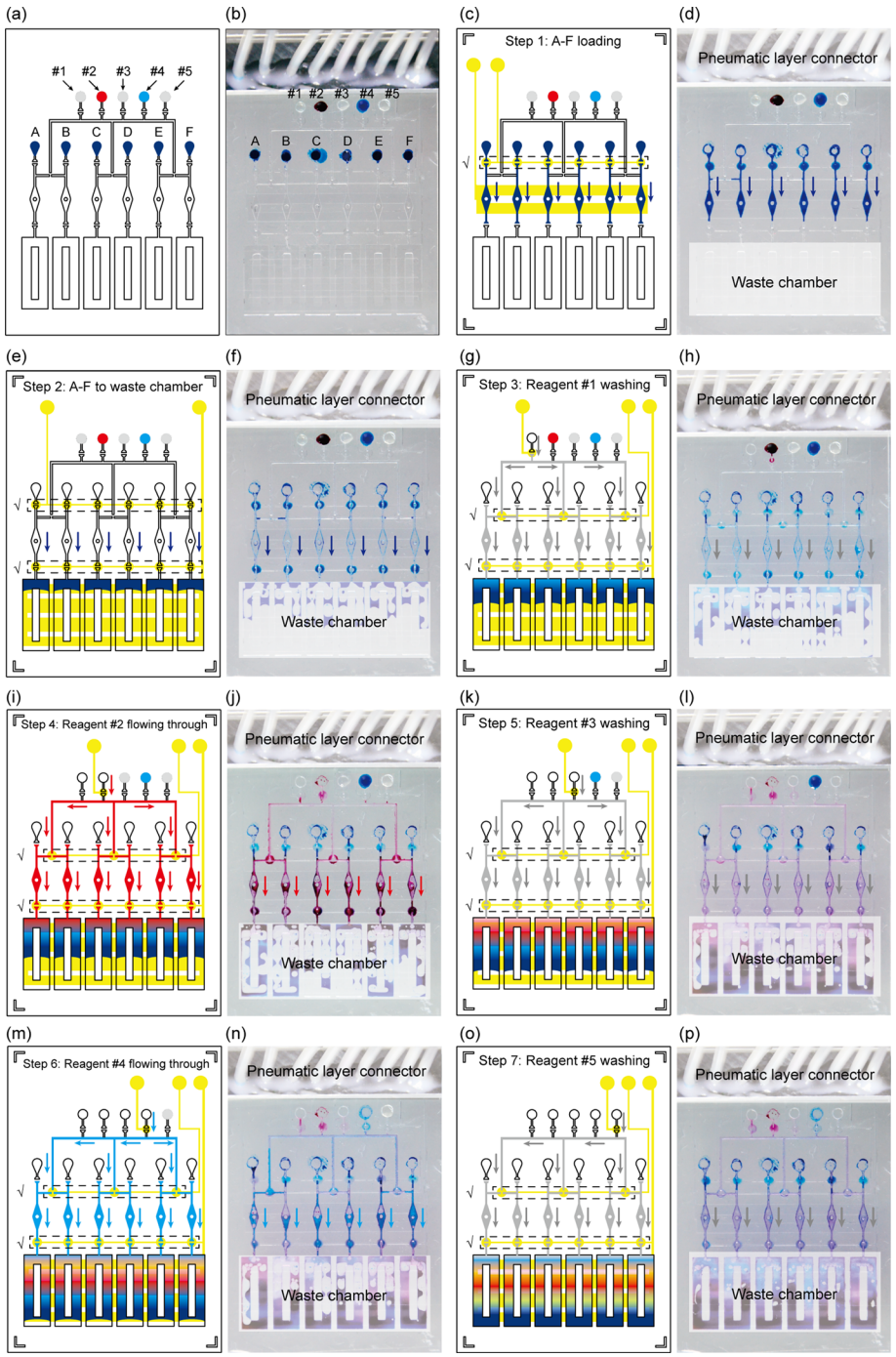

FIG. 6. Experimental tests of multiple step liquid sequential handling device. The device could automatically handle six samples and five reagents in seven steps. (a), (c), (e), (g), (i), (k), (m), (o) The schematics of the sequential handling procedure in each step. (b), (d), (f), (h), (J), (l), (n), (p) The experimental picture taken during the operation (chamber loadings, flowing "reactions," and washings). Reaction chamber color changing infers reaction/mixture between the dye molecules in the samples/reagents.

areas in the blue channel (Figs. 5(c) and 5(e)) means dense blue liquid in that area. Based on the comparison, it could be clearly seen that the liquids were well mixed in the serpentine channel, since uniform distributions of each color were observed in the later section of the channel in Figs. 5(e) and 5(f). As shown in Figs. 5(g) and 5(h), after the digitization, liquid volume in one hundred randomly chosen chambers are measured in Image J software (NIH) to evaluate

the digitization. The low deviation of liquid volume in these chambers (<2.5%, compared to the average value) infers the uniform distribution of mixed liquid sample in the isolated chambers that is crucial to the further quantitative nucleic acid amplification.

B. A multi-step sequential handling device for immunoassays

Immunoassays require multiple-step sequential processing of different fluid samples to quantitatively measure the concentration of target molecules, which leads to labor-intense, long-time duration procedures or expensive operation robots. The "gold standard" of immunoassays, the enzyme-linked immunosorbent assays (ELISAs), suggests that the actuation of sample loading, reactions, and washings according to the pre-set orders and time points is crucial to the accuracy of the assays. Herein, we designed a microfluidic chip to sequentially handle multiple fluids samples and reagents in an automatic manner, as the proof of the versatile usage of the mμSIP technique.

The tested microfluidic chip is connected to and driven by the miniature pressure source through a 9-channel pneumatic connector to automatically operate the liquid pumping and the flow control. The experimental results are demonstrated in Fig. 6. During the test, six liquid samples and five liquid reagents are pipetted into the inlets and then automatically handled by the system. The pressure source is programmed to a 7-step procedure, and for each step, the operation time is 5 min. In each step, there are different pneumatic branches being automatically activated by the vacuum pressure to actuate liquid pumping and to switch the microvalves, as depicted in Fig. 6.

Figs. 6(a) and 6(b) are the schematic illustration and the experimental picture of the microfluidic chip after pipetting the samples and the reagents. The dark bluer liquids represent samples A to F, and the other five different color liquids represent the reaction reagents #1 to #5 that are involved in the sequential procedures, as shown in Fig. 6(b). Among the reaction reagents, #1, #3, and #5 regents are clear-color DI water and #2 and #4 reagents are color dye solutions.

The first step is to load samples A to F into the reaction chambers for "incubation." During this step, the Nos. 1 and 2 pneumatic branches are activated by vacuum pressure, as illustrated in yellow in Fig. 6(c). The vacuum pressure in these two pneumatic channels switches on the diaphragm microvalves between the sample inlets and the reaction chambers, and as the result, samples A to F are pumped into the reaction chambers simultaneously, as shown in Fig. 6(d). It could be seen from the experiment picture that the reaction chamber is fully loaded with dark blue liquids without leaving any visible air bubbles.

The second step is to pump samples A to F into the waste chamber, as demonstrated in Figs. 6(e) and 6(f). In this step, the Nos. 2 and 9 pneumatic branches are exerted by the vacuum pressure (yellow in Fig. 6(e)), and the microvalves between the reaction chambers and the waste chambers are switched on to pump samples A to F to the waste chambers.

The third step is to wash the reaction chamber with a continuous flow of reagent #1, which is DI water, into the waste chamber, as shown in Figs. 6(g) and 6(h). In this step, the Nos. 3, 8, and 9 pneumatic branches are connected to the vacuum pressure (yellow in Fig. 6(g)), and the assisting microvalves are switched on to flow the DI water through the reaction chambers into the wastes, for washing. It could be seen that after this step of washing, the colors of the reaction chambers turned brighter than the colors before washing.

The fourth step is to pump the red reagent #2 through the reaction chambers for "reaction," as shown in Figs. 6(i) and 6(j). The Nos. 4, 8, and 9 pneumatic branches are activated by the vacuum pressure to load reagent #2 to flow through the chambers to the waste chambers (yellow in Fig. 6(i)). Fig. 6(j) is taken during the liquid flow, before all the liquids reach the waste chambers.

The following step of washing by #3 reagent, as the fifth step, removes the small amount of remaining red reagent #2. And the reaction chamber colors turn to light purple, as shown in Figs. 6(k) and 6(l).

The following steps, which are the sixth and the seventh steps, are to load reagents #4 and #5 through the reaction chamber in the designed orders, as shown in Figs. 6(i) to 6(p).

During the reagent flow through, the flow velocity of the reagents is tunable by varying the vacuum magnitude in the pressure source, to guarantee the sufficient reactions or washings. From the experiment pictures, it could be suggested that after each step, the colors of chambers change due to the reaction/mixture between the molecules in the dye solutions. Hence, it proves that the demonstrated device could handle the samples and reagents in the pre-set order to ensure the sequential processing that is of great significance in the immunoassays.

The demonstrated automatic microfluidic sequential flow system proves that mμSIP is not only able to actuate liquid pumping in an efficient, controllable, and bubble-free manner but also capable of minimizing the accessory flow control equipment and operation steps by integrating pneumatic valving structures. Further nucleic acid amplification or protein assay reaction that requires further surface modifications and feature device optimizations is not involved in this paper.

Both of the experiment characterizations and the demonstrated sequential fluid handling indicate that the mμSIP is potentially feasible for large-scale integration to build up microfluidic systems that implement versatile, complex, and precise functions, without redundant equipment.

V. CONCLUSIONS

In this paper, we present an automatic microfluidic sequential handling system, based on a bubble-free, tunable and mass production compatible liquid pumping method that is named mμSIP. The mμSIP is suitable for industrial manufacture since thermoplastics are used as major materials and the fabrication process is straightforward. The fluidic actuation mechanism can prevent the undesired air bubble formation intrinsically during liquid flow and is able to pump fluids into dead-end structures. Experimental characterizations suggested that by altering the major parameters, such as the air-permeable membrane thickness, the pneumatic channel coverage, and the vacuum pressure, the liquid flow rate could be well tuned, and a flow rate range of 0.013 μl/s to 0.097 μl/s was observed based on the tested design. The mμSIP consists of three layers of structure and is driven by vacuum pressure, so by introducing the pneumatic diaphragm microvalve, it can achieve unified pumping and control with minimal dependence on external equipment.

The demonstrated automatic sequential handling system, as the miniature pressure source and the microfluidic devices, could automatically process multiple fluids in the pre-set order for both potential digital nucleic acid assays and immunoassays. The system is easy to build up and to operate, and it also proves that it is an excellent option for complex and functional systems in future microfluidic assays and products. We hope this work to be beneficial and inspirational for further innovative microfluidic applications.

ACKNOWLEDGMENTS

The authors would like to thank Professor Luke P. Lee at the University of California, Berkeley, and his BioPOETS group for the discussion and help. The authors would like to thank Dr. John Waldeisen and Dr. Debkishore Mitra for the early discussions. This work was supported by the National Natural Science Foundation of China (NSFC No. 51175101) and the Programme of Introducing Talents of Discipline to Universities (Grant No. B07018).

[1]L. R. Volpatti and A. K. Yetisen, Trends Biotechnol. **32**(7), 347–350 (2014).
[2]M. A. Unger, H. P. Chou, T. Thorsen, A. Scherer, and S. R. Quake, Science **288**(5463), 113–116 (2000).
[3]T. Thorsen, S. J. Maerkl, and S. R. Quake, Science **298**(5593), 580–584 (2002).
[4]T. D. Wheeler and A. D. Stroock, Nature **455**(7210), 208–212 (2008).
[5]X. Yu, M. Hartmann, Q. Wang, O. Poetz, N. Schneiderhan-Marra, D. Stoll, C. Kazmaier, and T. O. Joos, PLos One **5**(10), e13125 (2010).
[6]C. H. Weng, K. Y. Lien, S. Y. Yang, and G. B. Lee, Microfluid. Nanofluid. **10**(2), 301–310 (2011).
[7]X. Zhang, Z. Chen, and Y. Huang, Biomicrofluidics **9**(1), 014118 (2015).

[8]R. Gorkin, J. Park, J. Siegrist, M. Amasia, B. S. Lee, J. M. Park, J. Kim, H. Kim, M. Madou, and Y. K. Cho, Lab Chip **10**(14), 1758–1773 (2010).
[9]A. Persat, R. D. Chambers, and J. G. Santiago, Lab Chip **9**(17), 2437–2453 (2009).
[10]A. Persat, M. E. Suss, and J. G. Santiago, Lab Chip **9**(17), 2454–2469 (2009).
[11]L. Y. Yeo and J. R. Friend, Biomicrofluidics **3**(1), 012002 (2009).
[12]H. A. Stone, A. D. Stroock, and A. Ajdari, Annu. Rev. Fluid Mech. **36**, 381–411 (2004).
[13]A. Gansen, A. M. Herrick, I. K. Dimov, L. P. Lee, and D. T. Chiu, Lab Chip **12**(12), 2247–2254 (2012).
[14]E. A. Ottesen, J. W. Hong, S. R. Quake, and J. R. Leadbetter, Science **314**(5804), 1464–1467 (2006).
[15]D. Juncker, H. Schmid, U. Drechsler, H. Wolf, M. Wolf, B. Michel, N. de Rooij, and E. Delamarche, Anal. Chem. **74**(24), 6139–6144 (2002).
[16]K. Hosokawa, K. Sato, N. Ichikawa, and M. Maeda, Lab Chip **4**(3), 181–185 (2004).
[17]C. D. Chin, V. Linder, and S. K. Sia, Lab Chip **12**(12), 2118–2134 (2012).
[18]I. K. Dimov, L. Basabe-Desmonts, J. L. Garcia-Cordero, B. M. Ross, A. J. Ricco, and L. P. Lee, Lab Chip **11**(5), 845–850 (2011).
[19]N. J. Cira, J. Y. Ho, M. E. Dueck, and D. B. Weibel, Lab Chip **12**(6), 1052–1059 (2012).
[20]H.-B. Liu, H.-Q. Gong, N. Ramalingam, Y. Jiang, C.-C. Dai, and K. M. Hui, J. Micromech. Microeng. **17**(10), 2055 (2007).
[21]T. Nakayama, Y. Kurosawa, S. Furui, K. Kerman, M. Kobayashi, S. R. Rao, Y. Yonezawa, K. Nakano, A. Hino, S. Yamamura, Y. Takamura, and E. Tamiya, Anal. Bioanal. Chem. **386**(5), 1327–1333 (2006).
[22]W. F. Zheng, Z. Wang, W. Zhang, and X. Y. Jiang, Lab Chip **10**(21), 2906–2910 (2010).
[23]E. Kang, D. H. Lee, C.-B. Kim, S. J. Yoo, and S.-H. Lee, J. Micromech. Microeng. **20**(4), 045009 (2010).
[24]S. Li, J. Liu, and D. Jiang, J. Heat Transfer **135**(9), 091403 (2013).
[25]C. Lochovsky, S. Yasotharan, and A. Gunther, Lab Chip **12**(3), 595–601 (2012).
[26]J. H. Kang, Y. C. Kim, and J. K. Park, Lab Chip **8**(1), 176–178 (2008).
[27]M. Kolnik, L. S. Tsimring, and J. Hasty, Lab Chip **12**(22), 4732–4737 (2012).
[28]C. Liu, J. A. Thompson, and H. H. Bau, Lab Chip **11**(9), 1688–1693 (2011).
[29]J. M. Karlsson, M. Gazin, S. Laakso, T. Haraldsson, S. Malhotra-Kumar, M. Maki, H. Goossens, and W. van der Wijngaart, Lab Chip **13**(22), 4366–4373 (2013).
[30]C. H. Zheng, J. W. Wang, Y. H. Pang, J. B. Wang, W. B. Li, Z. G. Ge, and Y. Y. Huang, Lab Chip **12**(14), 2487–2490 (2012).
[31]Y.-H. Lin, Y.-J. Chen, C.-S. Lai, Y.-T. Chen, C.-L. Chen, J.-S. Yu, and Y.-S. Chang, Biomicrofluidics **7**(2), 024103–024111 (2013).
[32]K. Eyer, S. Stratz, P. Kuhn, S. K. Küster, and P. S. Dittrich, Anal. Chem. **85**(6), 3280–3287 (2013).
[33]J. Melin and S. R. Quake, Annu. Rev. Biophys. Biomol. Struct. **36**, 213–231 (2007).
[34]P. Novo, F. Volpetti, V. Chu, and J. P. Conde, Lab Chip **13**(4), 641–645 (2013).
[35]S. J. Kim, S. Paczesny, S. Takayama, and K. Kurabayashi, Lab Chip **13**(11), 2091–2098 (2013).
[36]A. Apilux, Y. Ukita, M. Chikae, O. Chailapakul, and Y. Takamura, Lab Chip **13**(1), 126–135 (2013).
[37]S. M. Wang, L. Ge, X. R. Song, J. H. Yu, S. G. Ge, J. D. Huang, and F. Zeng, Biosens. Bioelectron. **31**(1), 212–218 (2012).
[38]C. Y. Li, C. Liu, Z. Xu, and J. M. Li, Microfluid. Nanofluid. **12**(5), 829–834 (2012).
[39]E. Fu, T. Liang, P. Spicar–Mihalic, J. Houghtaling, S. Ramachandran, and P. Yager, Anal. Chem. **84**(10), 4574–4579 (2012).
[40]L. Lafleur, D. Stevens, K. McKenzie, S. Ramachandran, P. Spicar-Mihalic, M. Singhal, A. Arjyal, J. Osborn, P. Kauffman, P. Yager, and B. Lutz, Lab Chip **12**(6), 1119–1127 (2012).
[41]W. S. Liu, D. L. Chen, W. B. Du, K. P. Nichols, and R. F. Ismagilov, Anal. Chem. **82**(8), 3276–3282 (2010).
[42]Y. J. Song, Y. Q. Zhang, P. E. Bernard, J. M. Reuben, N. T. Ueno, R. B. Arlinghaus, Y. L. Zu, and L. D. Qin, Nat. Commun. **3**, 1283 (2012).
[43]S. Begolo, D. V. Zhukov, D. A. Selck, L. Li, and R. F. Ismagilov, Lab Chip **14**(24), 4616–4628 (2014).
[44]D. B. Weibel, M. Kruithof, S. Potenta, S. K. Sia, A. Lee, and G. M. Whitesides, Anal. Chem. **77**(15), 4726–4733 (2005).
[45]J. Liu, D. Mitra, J. R. Waldeisen, R. H. Henrikson, Y. Park, S. Li, and L. P. Lee, paper presented at the 17th International Conference on Miniaturized Systems for Chemistry and Life Sciences, MicroTAS 2013, 27 October 2013–31 October 2013, Freiburg, Germany, 2013.
[46]K. J. Regehr, M. Domenech, J. T. Koepsel, K. C. Carver, S. J. Ellison-Zelski, W. L. Murphy, L. A. Schuler, E. T. Alarid, and D. J. Beebe, Lab Chip **9**(15), 2132–2139 (2009).
[47]E. Berthier, J. Warrick, H. Yu, and D. J. Beebe, Lab Chip **8**(6), 860–864 (2008).
[48]M. W. Toepke and D. J. Beebe, Lab Chip **6**(12), 1484–1486 (2006).
[49]W. H. Grover, R. H. C. Ivester, E. C. Jensen, and R. A. Mathies, Lab Chip **6**(5), 623–631 (2006).
[50]B. Vogelstein and K. W. Kinzler, Proc. Natl. Acad. Sci. U. S. A. **96**(16), 9236–9241 (1999).
[51]H. C. Fan, Y. J. Blumenfeld, Y. Y. El-Sayed, J. Chueh, and S. R. Quake, Am. J. Obstet. Gynecol. **200**(5), 543.e1–543.e7 (2009).
[52]M. Baker, Nat. Methods **9**(6), 541–544 (2012).
[53]See supplementary material at http://dx.doi.org/10.1063/1.4932303 for theoretical derivation, fabrication protocols and experiment observation description.